

# A Maximum Power Point Tracking of PV System by Adaptive Fuzzy Logic Control

Yuen-Haw Chang and Wei-Fu Hsu

**Abstract**—An adaptive fuzzy logic control (AFLC) for the maximum power point tracking (MPPT) algorithm is suggested in this paper. The AFLC is improved from scaling FLC, and it's mainly to adjust the duty-cycle of the defuzzification of FLC for facing many kinds of external variations, such as loading variation, current of solar cells. Here, our PV system is composed of solar cell, boost dc/dc converter, and AFLC controller for the goal of MPPT, and then we use OrCAD Pspice for the system simulation. The simulated cases via AFLC focus on the steady-state responses, and dynamic responses including loading variations and solar current change. The simulated results are illustrated to show the performances of the overall system.

**Index Terms**—maximum power point tracking (MPPT), Adaptive Fuzzy Logic Control (AFLC), photovoltaic (PV), boost DC/DC converter.

## I. INTRODUCTION

IN recent years, the energy crisis and environmental issues, such as air pollution and global warming effect, are driving research towards the development of renewable energy sources. In order to protect environment and get more energy available, the people always find new green energies, such as wind energy, water energy, solar energy...etc. Among them, the solar energy is now widely used, and it is a clean, maintenance-free, safe, and abundant resource of nature, so it is one of good green energy sources. But, there are still some problems: (i) The install cost of solar cells is higher. (ii) The conversion efficiency of PV system is lower. (iii) It is not a constant long-term energy because the sunlight intensity and temperature level of solar cells change anytime [1]. A PV module (composed of many solar cells in series/parallel) has the unique current versus voltage (I-V) characteristics [1, 2, 4]. From this characteristic, the power versus voltage (P-V) curve has a unique maximum power point (MPP) at a particular operating voltage and current. For any PV system, the output power can be increased by tracking the MPP by using a controller in a boost converter [3]. However, the MPP changes with sunlight intensity and temperature level due to the nonlinear characteristic of solar cells. Each type of solar cell has its own specific characteristic, so it leads to make the tracking of MPP more complicated. To overcome this problem, many MPPT algorithms have been presented

Manuscript received December 8, 2010. This work was supported in part by the National Science Council of Taiwan, R.O.C., under Grant NSC 99-2221-E-324-014. Yuen-Haw Chang and Wei-Fu Hsu are with the Department and Graduate Institute of Computer Science and Information Engineering, Chaoyang University of Technology, Taichung County, Taiwan, R.O.C. Post code: 413. (e-mail: [cyhfvc@cyut.edu.tw](mailto:cyhfvc@cyut.edu.tw), [s9827629@cyut.edu.tw](mailto:s9827629@cyut.edu.tw))

[1,2], and one of well-known algorithms is perturbation and observation algorithm (P&O algorithm) [4]. This P&O algorithm has the advantages of low cost and simple circuit. However, the steady-state oscillations often appear in P&O methods. Thus, it makes some power loss and slower tracking response.

In this paper, an adaptive FLC algorithm is suggested and modified as the basis of FLC. There are extra 4 adaptive rules to adjust the duty-cycle of the defuzzification for AFLC. It can not only reduce the time of tracking MPP, but also the regulation capability of MPPT is increased for the different number of solar cells (total current of PV module) or loading variation.

## II. MPPT FRAME OF PV SYSTEM

Fig.1 shows the MPPT frame of PV system. In this figure, there are three parts: (i) PV module, (ii) dc/dc converter, and (iii) AFLC controller for MPPT. Let's consider these parts as follows.

### A. PV Module

One cell of PV module we used is a low-power solar cell with open voltage  $V_{oc}=3.25V$  and normal rated current  $I_{rated}=100mA$ . In general, the equivalent models of solar cells have three types as in Fig. 2. Fig. 2(a) shows an ideal model with one current source and diode just. Fig. 2(b) has an extra small resistor to simulate the line loss. Fig. 2(c) has a big internal resistor to realize the solar cell's power loss. In this paper, we choose the model of Fig. 2(b) for the simulation later. Each solar cell has its own characteristic I-V curve. Of course,  $I_{PV}$  and  $V_{PV}$  change with sunlight intensity and temperature level, so does output power of PV module, where  $I_{PV}$  and  $V_{PV}$  are the total current and voltage of PV module, respectively. In Fig. 3, the dash lines show the I-V curves of a solar cell, and the real lines represent the P-V curves. It is obvious that each P-V curve for a specified  $I_{rated}$  has one MPP, e.g. MPP is located at  $Q(V_{mpp}, I_{mpp})$  as in Fig. 3.

### B. DC/DC Converter

The non-isolated boost converter is widely used in stand alone PV system, because it is simple, low cost, and high-efficiency. In general, the converter efficiency is closed to 90%. Here, we adopted the boost converter as our regulator [2]. In other words, we regulate properly the duty cycle of MOSFET SB of boost converter in order to change the operating point of  $I_{PV}$  and  $V_{PV}$ , so as to achieve MPPT.

### C. AFLC Controller for MPPT

The AFLC controller for MPPT is shown in the lower half of Fig.1, and it contains two parts: (i) fuzzy logic

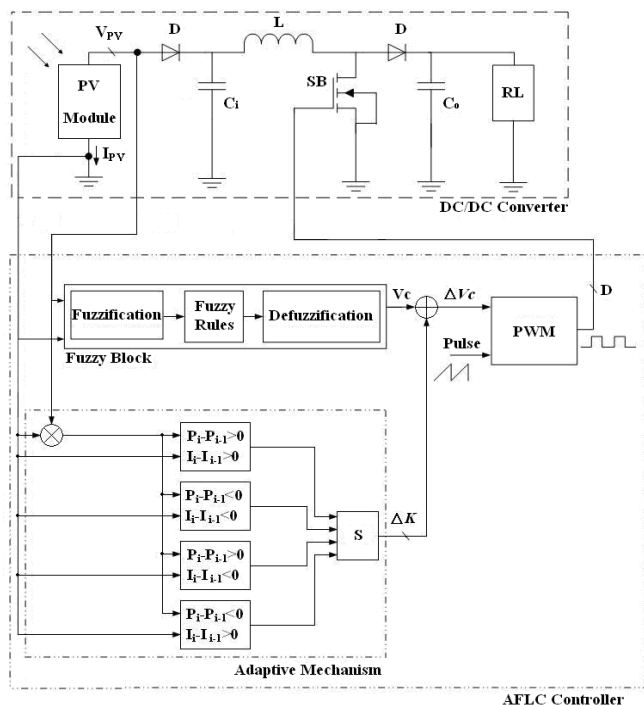


Fig. 1 MPPT frame of PV system

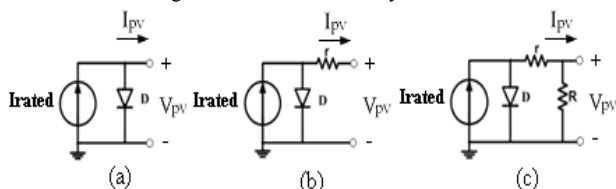


Fig.2 Solar Cell Model

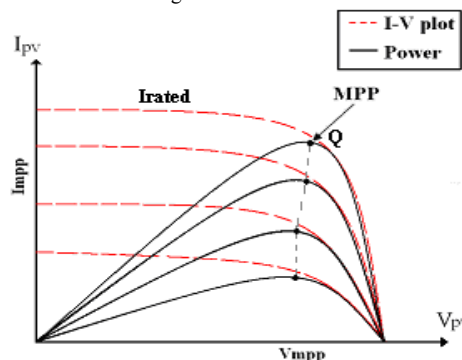


Fig.3 P-V Characteristic Curve of Solar Cell

control, (ii) adaptive mechanism. According to voltage ( $V_{pv}$ ) and current ( $I_{pv}$ ) of PV module in Fig. 1, the duty cycle  $D$  will be determined via AFLC controller in order to realize MPPT. The AFLC controller will be discussed further in the next section.

### III. CONTROLLER DESIGN

In this section, the AFLC controller for MPPT is discussed, and the goal is to improve the MPPT method of [7]. In general, the FLC is suitable to adjust the duty cycle of PV system when environment or load conditions have no big change. The reason is that  $I_{pv}$  and  $V_{pv}$  change slowly now. When environment or load conditions have big change, it is not enough just by using FLC to handle a big change of  $I_{pv}$  and  $P_{pv}$ . Thus, our suggestion is to add an adaptive mechanism into the FLC for meeting these problems. Here, the AFLC controller contains two parts: (i) fuzzy logic control, and (ii) adaptive mechanism described as follows.

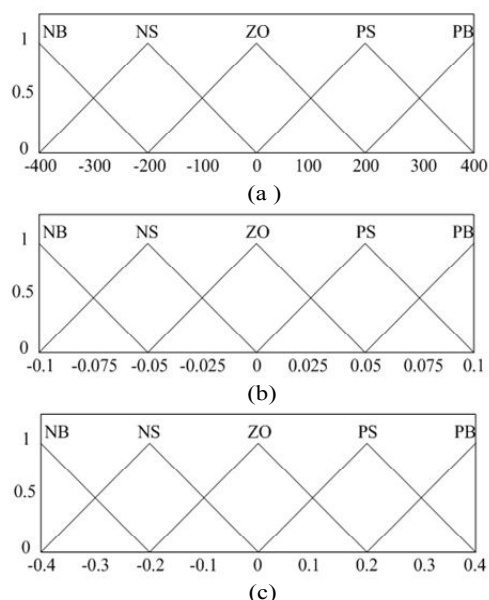


Fig.4 Membership Function (a) input  $I_{pv}(k)$ , (b) input  $V_{pv}(k)$ , (c) Duty cycle

Table 1 Fuzzy rules of AFLC

$I_{pv} \backslash V_{pv}$	NB	NS	ZO	PS	PB
NB	NB	NS	NS	ZO	ZO
NS	NS	ZO	ZO	ZO	PS
ZO	ZO	ZO	PS	PS	PS
PS	ZO	PS	PS	PS	PB
PB	PS	PS	PB	PB	PB

(i) Fuzzy logic control: The FLC is one part of AFLC, which is composed of three units: (a) fuzzification, (b) fuzzy rules, (c) defuzzification.

(a) Fuzzification: First,  $V_{pv}$  and  $I_{pv}$  of PV module are combined with the previous  $V_{pv}$  and  $I_{pv}$  for the averaged computation as:

$$V_{pv}(k) = [V_{pv}(k-1) + V_{pv}(k-2)]/2 \quad (1)$$

$$I_{pv}(k) = [I_{pv}(k-1) + I_{pv}(k-2)]/2 \quad (2)$$

Such an average is used for the local trend estimation of  $V_{pv}$  and  $I_{pv}$ . With the help of the trend estimation, the duty cycle can be obtained more effectively. Next, these voltage and current values are scaled and normalized into  $-400 \sim 400$  and  $-0.1 \sim 0.1$ , and through the membership function, the related fuzzy values ( $0 \sim 1$ ) can be estimated for each fuzzy descriptor: NB, NS, ZO, PS, and PB (e.g. NB: negative and big, ZO: zero, and PS: positive small) as shown in Fig.4. Finally, by comparing these values,  $V_{pv}$  and  $I_{pv}$  can be determined and assigned to the fuzzy descriptors (NB/NS/ZP/PS/PB), which have the biggest membership function values, respectively.

(b) Fuzzy rules: The syntax “if-then” is always used as the expressions of fuzzy rules, e.g. IF  $V_{pv}$  is PS and  $I_{pv}$  is NB, then  $D$  is ZO, i.e. when  $V_{pv}$  is PS and  $I_{pv}$  is NB, it means that  $V_{pv}$  is higher than the voltage  $V_{mpp}$  on MPP with a small current  $I_{pv}$ . We directly assign the duty cycle  $D$  to be ZO for the medium-sized drive, and it is enough to make the exceeded  $V_{pv}$  decreasing a little back to a suitable value.

**Table 2 Adaptive mechanism of AFLC**

Rule	$[P_{pv}(n) - P_{pv}(n-1)] > 0$	$[I_{pv}(n) - I_{pv}(n-1)] > 0$	Duty cycle	Select of $\Delta K$
(1)	truth	truth	decrease a little	K1
(2)	false	false		
(3)	truth	false	decrease a lot	K2
(4)	false	truth		

Here, for MPPT, we use 25 rules the totally. Table 1 shows the 25 fuzzy rules to define the relationship between  $V_{pv}$ ,  $I_{pv}$ , and  $D$ .

(c) Defuzzification: Defuzzification is for the aggregation of the  $D$  from each rule, i.e. the duty cycles from 25 rules must be computed and combined for a specified value. Here, we adopt the center of area (COA) defuzzification method as [8]:

$$V_c = \frac{\sum_{j=1}^{25} D_j(w_j) \cdot w_j}{\sum_{j=1}^{25} D_j(w_j)} \quad (3)$$

Where  $D_j$  is the duty cycle values for the  $j$ -th rule, and  $w_j$  is the weighted factor of the  $j$ -th rule. The  $w_j$  is bigger, the  $j$ -th rule affects more at this moment.

(ii) Adaptive mechanism: The purpose of the adaptive mechanism is to modify the duty cycle of the defuzzification of FLC, so it makes the PV system to provide a better response time and a higher output power. Here, the adaptive mechanism contains three parts as follows.

(a) First, in order to eliminate the high-frequency noise, we adopt the moving average filter to compute  $P_{PV}$  as:

$$P_{PV}(n) = [P_{pv}(n-1) + P_{pv}(n-2)]/2 \quad (4)$$

The moving average filter is a good way to estimate the local trend of the signal with possible high-frequency disturbances/noised. The basic ideal is by using the average computation of values within a moving window to estimate the trend change of the signal. Of course, the quality of trend estimation depends on the number of values within a window. Similarly, the sunlight intensity affects the current  $I_{PV}$  of PV module, so we adopt this method to estimate the trend of  $I_{pv}$  as:

$$I_{pv}(n) = [I_{pv}(n-1) + I_{pv}(n-2)]/2 \quad (5)$$

(b) Based on  $P_{PV}(n)$  and  $I_{PV}(n)$ , plus comparing with previous  $P_{PV}(n-1)$  and  $I_{PV}(n-1)$ , we can compute their differences. Then, it is obvious that the differences of  $P_{PV}$  and  $I_{PV}$  are either possible or negative, respectively. Thus, it can be summarized as 4 trends, and going a step further, 4 rules for adaptive mechanism can be suggested as shown in Table 2. Let's explain these rules as follows.

(1) Rule 1 and Rule 2: A fixed parameter is inadequate in applications when the operating conditions have change, and it is not reliable. Thus, the duty cycle can be modified by rule 1 and rule 2, and then the adaptive

value  $\Delta K$  is assigned to  $K1=-0.25$ . Because  $\Delta K$  is a smaller negative value now, the duty cycle will be modified to decrease a little.

(2) Rule 3 and Rule 4: Similarly, the duty cycle can be modified by rule 3 and rule 4, and then the adaptive value  $\Delta K$  is assigned to  $K2=-0.3$ . Because  $\Delta K$  is a bigger negative value now, the duty cycle will be modified to decrease a lot.

(c) To combine this adaptive value  $\Delta K$  and  $V_c$  from defuzzification, the duty-cycle control voltage  $\Delta V_c$  can be obtained as:

$$\Delta V_c = V_c + \Delta K \quad (6)$$

By using the  $\Delta V_c$ , the duty cycle  $D$  is determined via the PWM block as in Fig. 1 for the control of MOSFET SB so as to realize the MPP search.

#### IV. SIMULATION OF MPPT BY AFLC

In this section, the PV system with AFLC is designed and simulated by using OrCAD Pspice based on the scheme in Fig. 1, and then the results will be compared with those by scaling FLC. Here, a PV module contains 1~10 solar cells in parallel (10 at most), and each solar cell has  $V_{oc}=3.25V$  (open voltage) and  $I_{rated}=100mA$  (rated current). In general, the solar voltage of MPP is at 70%~82% of  $V_{oc}$ , and the solar current at MPP is close to about 86% of  $I_{rated}$ . According to [6], we can calculate the minimum/ maximum MPP of a solar cell as follows:

$$P_{min} = 0.7V_{OC} \times 0.86 I_{rated} \quad (7)$$

$$P_{max} = 0.82V_{OC} \times 0.86 I_{rated} \quad (8)$$

Based on (7) and (8), the minimum value of MPP is estimated about 194.79mW, and the maximum is about 229.19mW. A DC/DC boost converter is operated at the switching frequency of 60 kHz, and all components are listed as follows:  $R_L=30\Omega$ ,  $C_i=10000\mu F$  (10 solar cells)  $C_o=200\mu F$ ,  $L=100\mu H$ , and MOSFET=IRF450. Here, the simulation cases include: (i) steady-state response, (ii) dynamic response to variation of  $R_L$ , (iii) dynamic response to variation of  $I_{PV}$ , (iv) dynamic response to variation of  $R_L$  and  $I_{PV}$  at the same time.

(i) Firstly, the steady-state response is discussed here ( $C_i=1000\mu F$ ). When a single solar cell is working, the PV system can be simulated to obtain the waveforms of  $V_{PV-t}$ ,  $P_{PV-t}$ ,  $I_{PV-t}$ ,  $P_{PV-V_{PV}}$ , and  $I_{PV-V_{PV}}$ . The AFLC simulation result is shown in Fig. 5(a), and clearly, the final value of  $P_{PV}$  is reaching 221mW after 44ms. Fig. 5(b) shows the curves of  $P_{PV-V_{PV}}$  and  $I_{PV-V_{PV}}$  of AFLC, and it is found that the voltage on MPP ( $V_{PV}=2.32V$ ) is at about 71% of  $V_{oc}$ , and the MPP search can be realized now. The FLC simulation result is shown in Fig. 6(a), and the final value of  $P_{PV}$  is reaching 218mW after 61ms. Fig. 6(b) shows curves of  $P_{PV-V_{PV}}$  and  $I_{PV-V_{PV}}$  by FLC, and it is found that the voltage on MPP ( $V_{PV}=2.27V$ ) is at about 70% of  $V_{oc}$ . From the above results for a solar cell as in Fig. 5 and Fig. 6, it can be observed that the output power by using AFLC is higher than that only by FLC, and the response time by AFLC is faster than that by FLC. Next, when 10 solar cells are working in parallel, the PV system can be simulated to obtain the waveforms of  $V_{PV-t}$ ,  $P_{PV-t}$ ,  $I_{PV-t}$ ,  $P_{PV-V_{PV}}$ , and

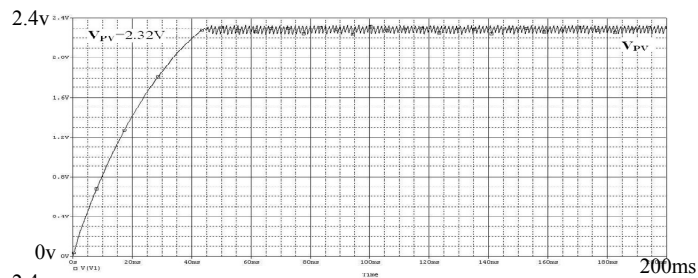


Fig. 5(a)  $V_{PV}$ -t,  $P_{PV}$ -t, and  $I_{PV}$ -t by AFLC (one solar cell)

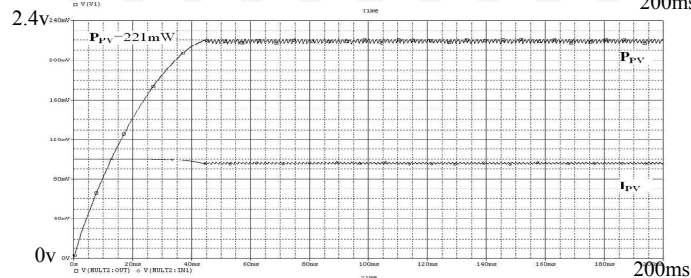


Fig. 5(b)  $P_{PV}$ - $V_{PV}$  and  $I_{PV}$ - $V_{PV}$  by AFLC (one solar cell)

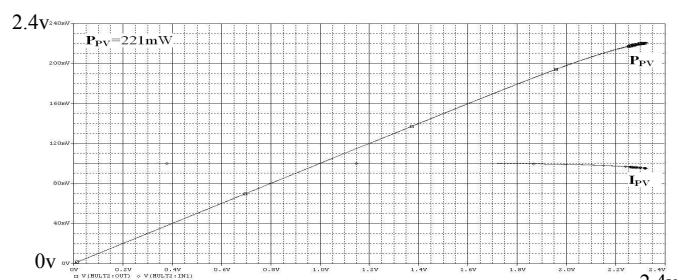


Fig. 6(a)  $V_{PV}$ -t,  $P_{PV}$ -t, and  $I_{PV}$ -t by FLC (one solar cell)

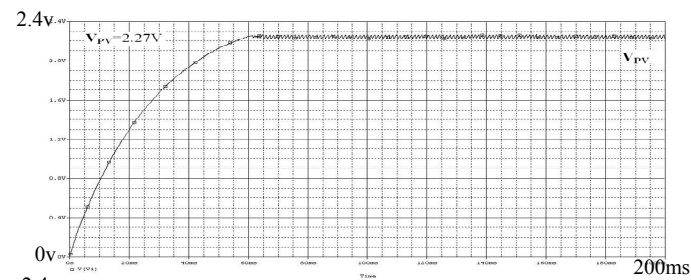


Fig. 6(b)  $P_{PV}$ - $V_{PV}$  and  $I_{PV}$ - $V_{PV}$  by FLC (one solar cell)

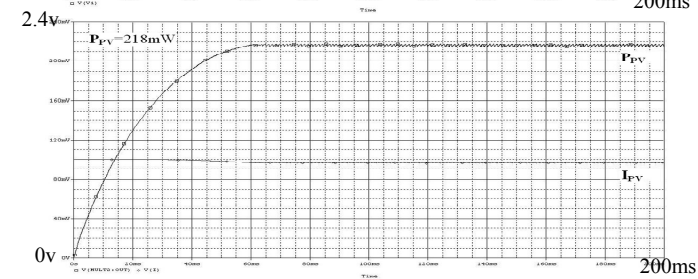


Fig. 7(a)  $V_{PV}$ -t,  $P_{PV}$ -t, and  $I_{PV}$ -t by AFLC (10 solar cells)

$I_{PV}$ - $V_{PV}$ . The AFLC simulation result is shown in Fig. 7(a), and the final value of  $P_{PV}$  is reaching 2.06W after 24ms. Fig. 7(b) shows curves of  $P_{PV}$ - $V_{PV}$  and  $I_{PV}$ - $V_{PV}$  by AFLC. The FLC simulation result is shown in Fig. 8(a), and the final value of  $P_{PV}$  is reaching 2.06W after 24.3ms. Fig. 8(b) shows curves of  $P_{PV}$ - $V_{PV}$  and  $I_{PV}$ - $V_{PV}$  by FLC. From the above results for 10 solar cells as in Fig. 7-8, it is obvious that output power by AFLC is close to that only by FLC, but the response time by AFLC is still faster than that by FLC.

(ii) Secondly, the dynamic response to the variation of RL is discussed here ( $C_i=1000\mu F$ ). When a signal solar cell is working, RL suddenly changes from  $30\Omega$  to  $15\Omega$  at 100ms, and recovers from  $15\Omega$  back to  $30\Omega$  at 200ms. For such the variation of RL, the PV system is simulated for

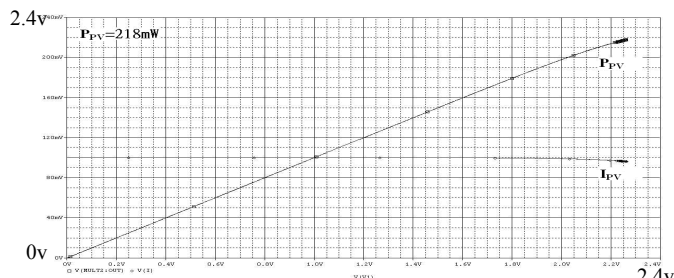


Fig. 7(b)  $P_{PV}$ - $V_{PV}$  and  $I_{PV}$ - $V_{PV}$  by FLC (one solar cell)

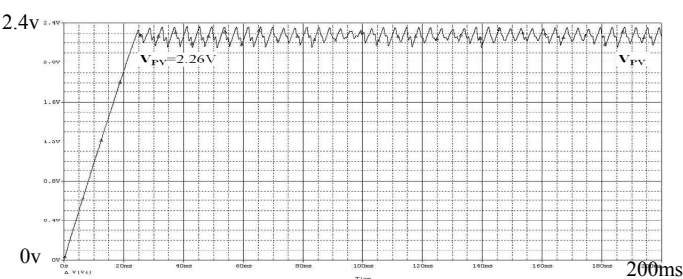


Fig. 7(a)  $V_{PV}$ -t,  $P_{PV}$ -t, and  $I_{PV}$ -t by AFLC (10 solar cells)

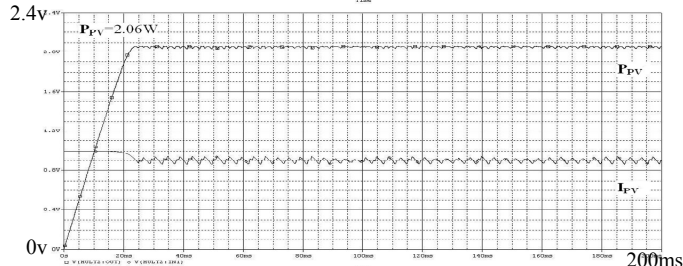


Fig. 7(b)  $P_{PV}$ - $V_{PV}$  and  $I_{PV}$ - $V_{PV}$  by AFLC (10 solar cells)

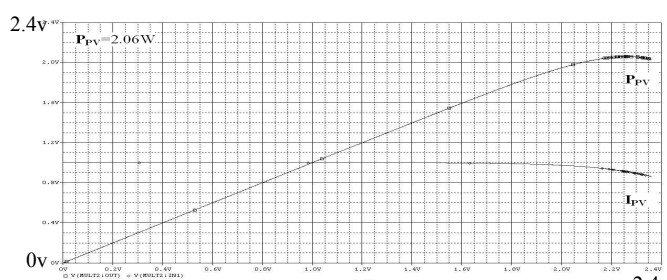


Fig. 8(a)  $V_{PV}$ -t,  $P_{PV}$ -t, and  $I_{PV}$ -t by FLC (10 solar cells)

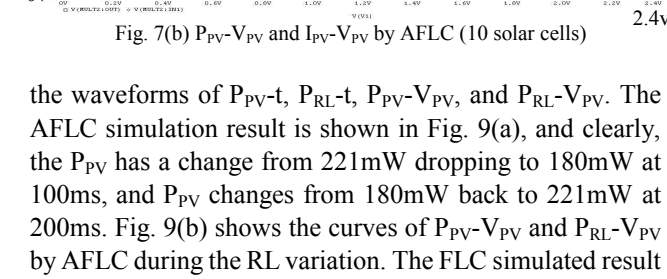


Fig. 8(b)  $P_{PV}$ - $V_{PV}$  and  $I_{PV}$ - $V_{PV}$  by FLC (10 solar cells)

the waveforms of  $P_{PV}$ -t,  $P_{RL}$ -t,  $P_{PV}$ - $V_{PV}$ , and  $P_{RL}$ - $V_{PV}$ . The AFLC simulation result is shown in Fig. 9(a), and clearly, the  $P_{PV}$  has a change from 221mW dropping to 180mW at 100ms, and  $P_{PV}$  changes from 180mW back to 221mW at 200ms. Fig. 9(b) shows the curves of  $P_{PV}$ - $V_{PV}$  and  $P_{RL}$ - $V_{PV}$  by AFLC during the RL variation. The FLC simulated result is shown in Fig. 10(a), and clearly, the  $P_{PV}$  has a change from 218mW dropping to 147mW at 100ms, and  $P_{PV}$  changes from 147mW back to 218mW at 200ms. Fig. 10(b) shows the curve of  $P_{PV}$ - $V_{PV}$  and  $P_{RL}$ - $V_{PV}$  by FLC during the RL variation. From the above results, it is obvious that the output power by AFLC is higher than that by FLC, and the response time by AFLC is faster than that by FLC.

(iii) Thirdly, the dynamic response to the variation of  $I_{PV}$  is discussed here. Now assume that  $I_{PV}$  suddenly changes from 1A to 100mA at 100ms, and recovers from 100mA back to 1A at 200ms. For such the variation of  $I_{PV}$ , the PV system can be simulated to obtain the waveforms of  $P_{PV}$ -t,  $I_{PV}$ -t,  $P_{PV}$ - $V_{PV}$ , and  $I_{PV}$ - $V_{PV}$ . The AFLC simulation result is shown in Fig. 11(a), and clearly, the  $P_{PV}$  has a change from 2.34W dropping to 220mW at 100ms, and  $P_{PV}$  changes from 220mW back to 2.34W at 200ms. Fig. 11(b) shows the curves of  $P_{PV}$ - $V_{PV}$  and  $I_{PV}$ - $V_{PV}$  by AFLC during the  $I_{PV}$

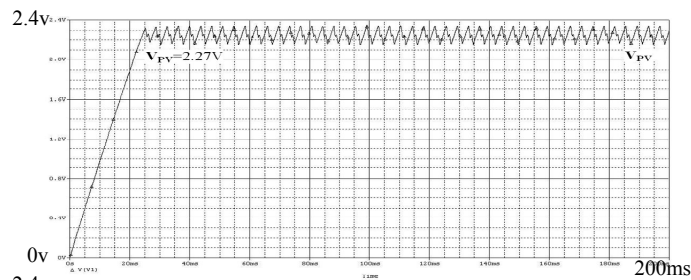


Fig. 8(a)  $V_{PV}$ -t,  $P_{PV}$ -t, and  $I_{PV}$ -t by FLC (10 solar cells)

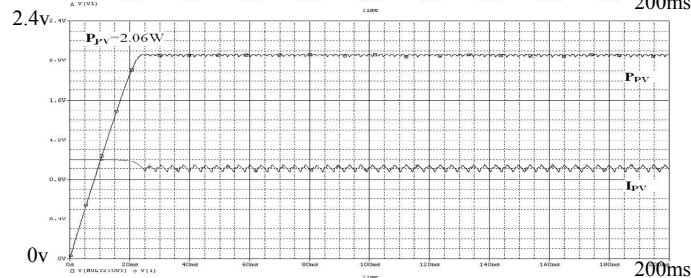


Fig. 8(b)  $P_{PV}$ - $V_{PV}$  and  $I_{PV}$ - $V_{PV}$  by FLC (10 solar cells)

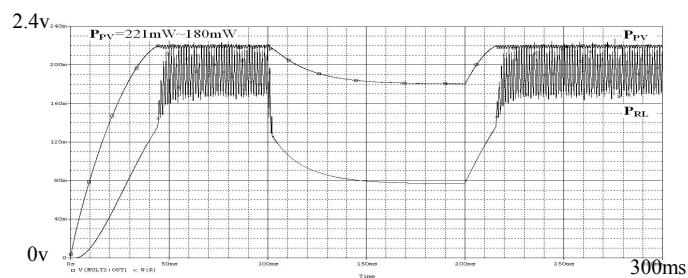


Fig. 9(a)  $P_{PV}$ -t, and  $P_{RL}$ -t by AFLC (RL=30Ω to 15Ω)

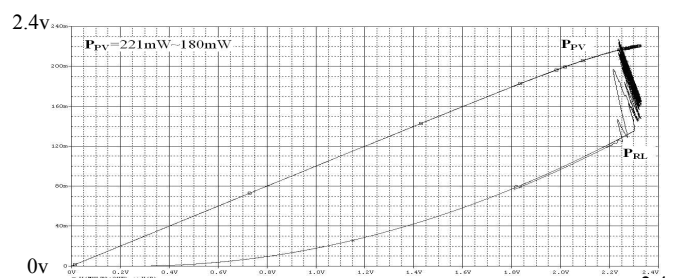


Fig. 9(b)  $P_{PV}$ - $V_{PV}$  and  $P_{RL}$ - $V_{PV}$  by AFLC (RL=30Ω to 15Ω)

variation. The FLC simulated result is shown in Fig. 12(a), and clearly, the  $P_{PV}$  has a change from 2.32W dropping to 217mW at 100ms, and  $P_{PV}$  changes from 217mW back to 2.32W at 200ms. Fig. 12(b) shows the curves of  $P_{PV}$ - $V_{PV}$  and  $I_{PV}$ - $V_{PV}$  by FLC during the  $I_{PV}$  variation. From the above results, it is obvious that the output power by AFLC is higher than that by FLC, and the response time by AFLC is also faster than that by FLC.

(iv) Finally, the dynamic response to the variations of  $I_{PV}$  and RL at the same time is discussed here. The  $I_{PV}$  changes from 1A to 100mA, and RL changes from 30Ω to 15Ω at 100ms, and then at 200ms,  $I_{PV}$  recovers from 100mA back to 1A, and RL is from 15 Ω back to 30Ω. For these variation

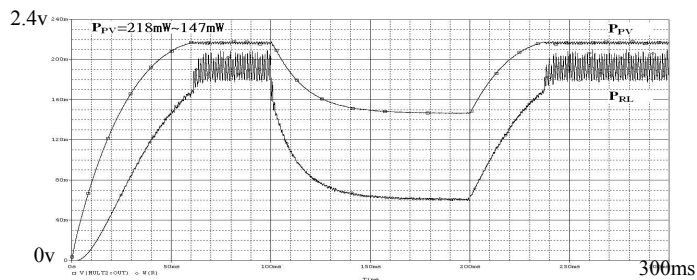


Fig. 10(a)  $P_{PV}$ -t, and  $P_{RL}$ -t by FLC (RL=30Ω to 15Ω)

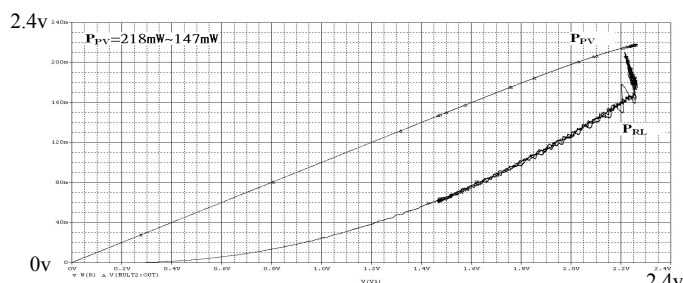


Fig. 10(b)  $P_{PV}$ - $V_{PV}$  and  $P_{RL}$ - $V_{PV}$  by FLC (RL=30Ω to 15Ω)

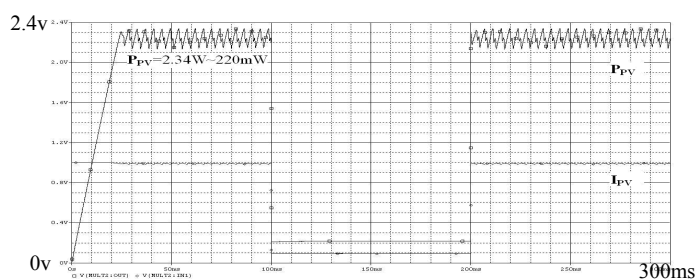


Fig. 11(a)  $P_{PV}$ -t, and  $I_{PV}$ -t by AFLC ( $I_{PV}$ =1A to 100mA)

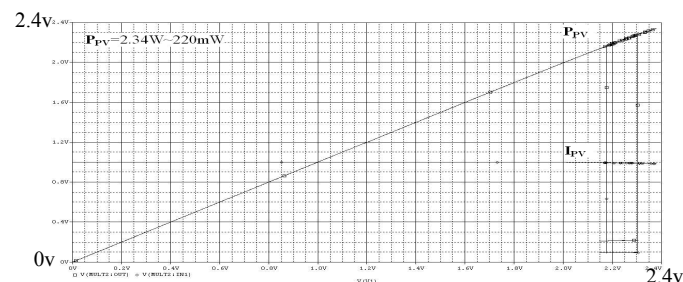


Fig. 11(b)  $P_{PV}$ - $V_{PV}$  and  $I_{PV}$ - $V_{PV}$  by AFLC ( $I_{PV}$ =1A to 100mA)

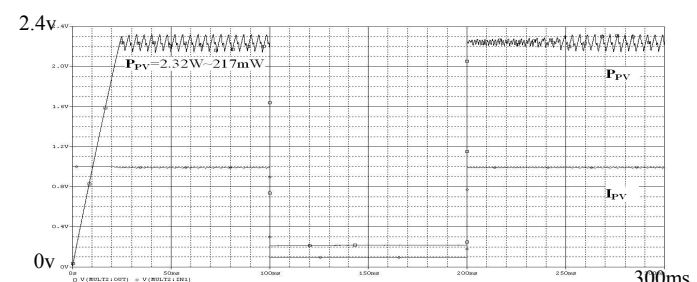


Fig. 12(a)  $P_{PV}$ -t, and  $I_{PV}$ -t by FLC ( $I_{PV}$ =1A to 100mA)

of  $I_{PV}$  and RL, the PV system can be simulated to obtain the waveforms of  $P_{PV}$ -t,  $P_{RL}$ -t,  $I_{PV}$ -t,  $P_{PV}$ - $V_{PV}$ ,  $P_{RL}$ - $V_{PV}$ , and  $I_{PV}$ - $V_{PV}$ . The AFLC simulation result is shown in Fig. 13(a), and clearly, the  $P_{PV}$  has a change from 2.34W dropping to 202mW at 100ms, and  $P_{PV}$  changes from 202mW back to 2.34W at 200ms. Fig. 13(b) shows the curves of  $P_{PV}$ - $V_{PV}$ ,  $P_{RL}$ - $V_{PV}$ , and  $I_{PV}$ - $V_{PV}$  by AFLC during the  $I_{PV}$  and RL variations at the same time. The FLC simulated result is shown in Fig. 14(a), and clearly, the  $P_{PV}$  has a change from 2.32W dropping to 180mW at 100ms, and  $P_{PV}$  changes from 180mW back to 2.32W at 200ms. Fig. 14(b) shows the curves of  $P_{PV}$ - $V_{PV}$ ,  $P_{RL}$ - $V_{PV}$ , and  $I_{PV}$ - $V_{PV}$  by FLC during the

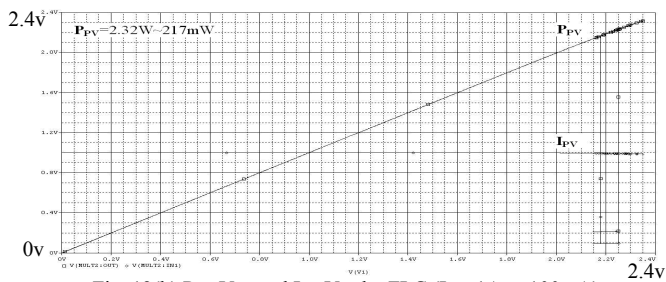


Fig. 12(b)  $P_{PV}$ - $V_{PV}$  and  $I_{PV}$ - $V_{PV}$  by FLC ( $I_{PV}=1A$  to  $100mA$ )

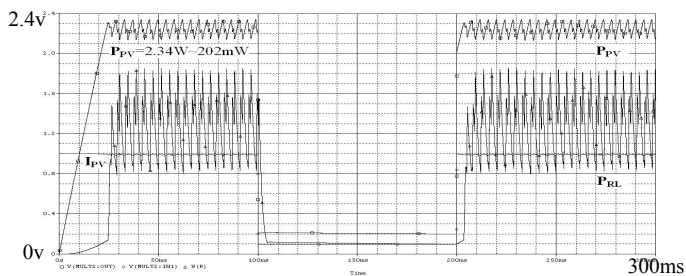


Fig. 13(a)  $P_{PV}$ - $t$ ,  $P_{RL}$ - $t$ , and  $I_{PV}$ - $t$  by AFLC ( $I_{PV}=1A$  to  $100mA$ ,  $R_L=30\Omega$  to  $15\Omega$ )

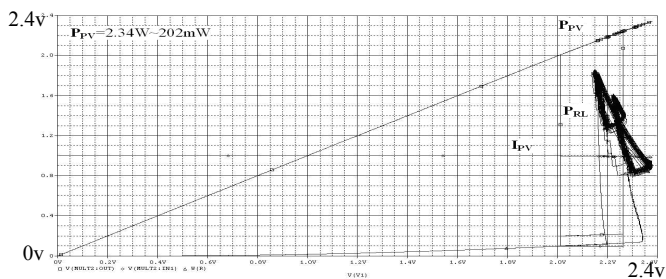


Fig. 13(b)  $P_{PV}$ - $V_{PV}$ ,  $P_{RL}$ - $V_{PV}$ , and  $I_{PV}$ - $V_{PV}$  by AFLC ( $I_{PV}=1A$  to  $100mA$ ,  $R_L=30\Omega$  to  $15\Omega$ )

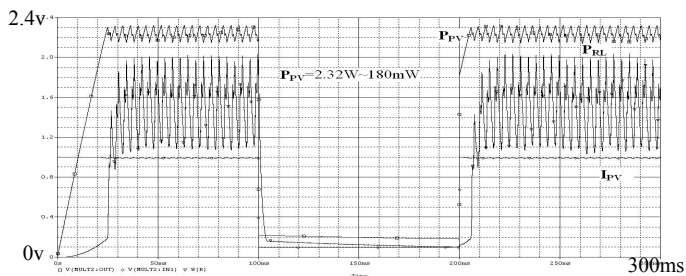


Fig. 14(a)  $P_{PV}$ - $t$ ,  $P_{RL}$ - $t$ , and  $I_{PV}$ - $t$  by FLC ( $I_{PV}=1A$  to  $100mA$ ,  $R_L=30\Omega$  to  $15\Omega$ )

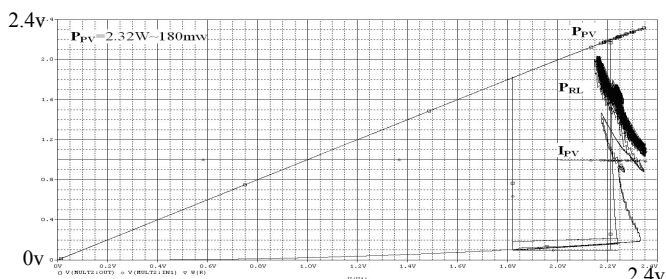


Fig. 14(b)  $P_{PV}$ - $V_{PV}$ ,  $P_{RL}$ - $V_{PV}$ , and  $I_{PV}$ - $V_{PV}$  by FLC ( $I_{PV}=1A$  to  $100mA$ ,  $R_L=30\Omega$  to  $15\Omega$ )

$I_{PV}$  and  $R_L$  variations at the same time. From the above results, it is obvious that the output power by AFLC is higher than that by FLC, and the response time by AFLC is faster than that by FLC.

### V. CONCLUSION

An AFLC for the MPPT algorithm is suggested in this paper. The AFLC is modified from scaling FLC, and the



Fig.15 Hardware of PV System for MPPT

goal is to improve the MPPT method of [7]. The AFLC controller is realized and tested for realizing MPPT as single or 10 solar cells. Comparing the results between AFLC and scaling FLC, the former has the better performance of steady-state/dynamic response. The AFLC has not only improved the response time of PV system, but also provided to track the higher output power of PV system. At present, we have implemented the hardware of PV System for MPPT as shown the photo in Fig. 15. Next, some more experimental results will be measured for the verification of this scheme.

### REFERENCES

- [1] V.Salas, E.Olyas, A.Barrado, A. Lazaro, "Review Of The Maximum Power Point Tracking Algorithms For Stand-Alone Photovoltaic Systems", *Solar Energy Materials & Solar Cells*, Vol. 90, 2006, pp.1555-1578.
- [2] N. Ozog, W. Xiao, and W. G. Dunford, "Topology study of photovoltaic interface for maximum power point tracking," *IEEE Trans. Ind. Electron.*, vol. 54, no. 3, pp. 1696-1704, Jun. 2007.
- [3] J. L. Santos, F. Antunes, A. Chehab And C. C. Cruz, "A Maximum Power Point Tracker For PV Systems Using A High Performance Boost Converter", *Solar Energy*, vol. 80, 2006 , pp. 772-778.
- [4] T. Taficht, K. Agbossou, M.L. Doumbia, A. Chériti "An improved maximum power point tracking method for photovoltaic systems", *Renewable Energy*, Volume 33, Issue 7, July 2008, Pages 1508-1516.
- [5] Nopporn Patcharaprakiti, Suttichai Premrudeepreechacharn, Yosana Sriuthaisiriwong "maximum power point tracking using adaptive fuzzy logic control for grid-connected photovoltaic system", *Renewable Energy*, Volume 30, Issue 11, September 2005, Pages 1771-1788
- [6] H. L. Hey, J. D. P. Pacheco, J. Imhoff, and R. Gules, "A maximum power point tracking system with parallel connection for PV stand-alone applications," *IEEE Trans. Ind. Electron.*, vol. 55, no. 7, pp. 2674-2683, Jul. 2008.
- [7] Yuen-Haw Chang, and Chia-Yu Chang, "A Maximum Power Point Tracking of PV System by Scaling Fuzzy Control," IMECS 2010, March 17-19,2010, Hong Kong.
- [8] C. Lee, "Fuzzy logic in control systems: Part I and part II," *IEEE Trans. Syst., Man, Cybern.*, vol. 20, no. 2, pp. 404-435, Mar.-Apr. 1990.